

The nature of lunar volatiles as revealed by Mini-RF observations of the LCROSS impact site

C. D. Neish,¹ D. B. J. Bussey,¹ P. Spudis,² W. Marshall,^{3,4} B. J. Thomson,¹ G. W. Patterson,¹ and L. M. Carter⁵

Received 7 May 2010; revised 13 August 2010; accepted 14 October 2010; published 13 January 2011.

[1] On 9 October 2009 the Lunar Crater Observation and Sensing Satellite (LCROSS) impacted Cabeus crater, located near the south pole of the Moon. Prior to that impact, the Mini-RF instruments on ISRO's Chandrayaan-1 and NASA's Lunar Reconnaissance Orbiter (LRO) obtained S band (12.6 cm) synthetic aperture radar images of the impact site at 150 and 30 m resolution, respectively. These observations show that the floor of Cabeus has a circular polarization ratio (CPR) comparable to or less than the average of nearby terrain in the southern lunar highlands. Furthermore, <2% of the pixels in Cabeus crater have CPR values greater than unity. This observation is not consistent with the presence of thick deposits of nearly pure water ice within a few meters of the lunar surface, but it does not rule out the presence of small (<~10 cm), discrete pieces of ice mixed in with the regolith. In addition, Mini-RF on LRO acquired a postimpact S band image of the region surrounding the LCROSS impact site, providing important geologic context for the site. Registering the LRO image to a near-infrared (NIR) image taken by the LCROSS shepherding spacecraft, we find that the impactor landed in the ray of a fresh, radar-bright, 1 km crater. However, the difference between preimpact and postimpact images is not above the speckle noise. This implies that the size of the LCROSS impact crater is less than Mini-RF's resolution (30 m), and/or that the impact did not excavate more decimeter-size blocks than were already present at the impact site.

Citation: Neish, C. D., D. B. J. Bussey, P. Spudis, W. Marshall, B. J. Thomson, G. W. Patterson, and L. M. Carter (2011), The nature of lunar volatiles as revealed by Mini-RF observations of the LCROSS impact site, *J. Geophys. Res.*, 116, E01005, doi:10.1029/2010JE003647.

1. Introduction

[2] On 9 October 2009 the Lunar Crater Observation and Sensing Satellite (LCROSS) Centaur stage and shepherding spacecraft impacted Cabeus crater, located near the south pole of the Moon [Colaprete *et al.*, 2010]. The LCROSS mission objective was to identify the source of the elevated hydrogen observed at the poles of the Moon by the Lunar Prospector neutron spectrometer [Feldman *et al.*, 1998]. Water, which is one source of that hydrogen, can be brought to the Moon by comets and asteroids, be formed through reactions between the lunar soil and solar wind implanted hydrogen, or be outgassed from the lunar interior over billions of years [Watson *et al.*, 1961; Arnold, 1979]. This

water can then migrate through ballistic trajectories with eventual capture in permanently shadowed regions near the poles of the Moon [Arnold, 1979], some of which have annual averaged temperatures less than 40 K [Paige *et al.*, 2010]. Losses due to meteoritic bombardment [Arnold, 1979], erosion by solar wind sputtering [Lanzerotti *et al.*, 1981], or photodissociation [Morgan and Shemansky, 1991] may exceed the accretion rate of water, however, impeding the formation of ice deposits in the polar cold traps. Thus, determining the form and the amount of water ice in permanently shadowed areas such as that found in Cabeus crater would put constraints on models of the impact history of the lunar surface, and the importance of the different water delivery and loss processes.

[3] Equipped with its own active source, a synthetic aperture radar (SAR) is one of few instruments that can “see in the dark”. This allows it to view areas of permanent shadow near the poles of the Moon. Thick deposits of nearly pure water ice have an unusual radar signature that would be observable with such an instrument. When an incident circularly polarized radar wave is backscattered off an interface, the polarization state of the wave changes. For most surfaces, this leads to a return with more of an “opposite

¹Johns Hopkins University Applied Physics Laboratory, Laurel, Maryland, USA.

²Lunar and Planetary Institute, Houston, Texas, USA.

³Universities Space Research Association, Mountain View, California, USA.

⁴NASA Ames Research Center, Moffett Field, California, USA.

⁵NASA Goddard Space Flight Center, Greenbelt, Maryland, USA.

sense” (OC) polarization than a “same sense” (SC) polarization, so the circular polarization ratio (CPR = SC/OC) remains less than 1. However, in weakly absorbing media (such as water ice) the radar signal can undergo a series of forward scattering events off small imperfections in the material, each of which preserves the polarization properties of the signal [Peters, 1992; Hagfors et al., 1997]. Those portions of the wavefront that are scattered along the same path but in opposite directions combine coherently to produce an increase in the SC radar backscatter [Hapke, 1990]. This coherent backscatter effect leads to large returns in the same sense (SC) polarization and values for CPR that can exceed unity. Note that $CPR > 1$, while diagnostic of water ice, is not a unique signature for water ice. Very rough, dry surfaces have also been observed to have CPRs that exceed unity [e.g., Campbell et al., 1993, 1999]. The CPR may increase in such regions due to double-bounce scattering between the surface and rock faces [Campbell et al., 2009].

[4] The coherent backscatter effect has been observed on the Galilean satellites [e.g., Ostro et al., 1992], Mars’ polar ice caps [e.g., Muhleman et al., 1991], and in craters near the poles of Mercury [e.g., Slade et al., 1992; Harmon et al., 2001]. This latter observation suggests the presence of nearly pure water ice in polar cold traps on Mercury, lending credence to the idea that similar deposits could exist on the Moon. Nozette et al. [1996] reported an increased SC radar return over Shackleton crater near the south pole of the Moon, but their inference of ice was not supported by Stacy et al. [1997] and Campbell et al. [2006] in their interpretation of subsequent, higher-resolution polarimetric imaging of shadowed crater floors. More recently, radar observations of the north pole of the Moon have revealed intriguing areas of high CPR that warrant further study [Spudis et al., 2010].

[5] Early reports from the LCROSS team indicate a discovery of water in Cabeus crater [Colaprete et al., 2010]. In particular, the down-looking near-infrared spectrometer on the LCROSS shepherding spacecraft observed absorptions due to water vapor and ice particles after the Centaur impacted the lunar surface. SAR observations provide constraints on the form of that water. For example, if the water were in the form of a thick deposit of nearly pure ice under a thin layer of regolith, it would be observable by radar. In this situation, the coherent backscatter effect would cause large enhancements in SC radar backscatter and CPR. If, on the other hand, the water were in the form of small grains of ice mixed into the regolith, it would be difficult to distinguish from a rocky surface. The change in dielectric constant caused by the presence of a small concentration of water ice would not produce large scattering differences [Thompson et al., 2010].

[6] In November 2008, the Indian Space Research Organization (ISRO) launched the Chandrayaan-1 spacecraft carrying a Mini-SAR instrument [Nozette et al., 2010]. This instrument (dubbed “Forerunner”) was capable of obtaining SAR images at 150 m resolution in the S band (12.6 cm). Before the spacecraft’s demise in August 2009, Forerunner acquired nearly complete (>90% coverage) mosaics of both polar regions of the Moon [Spudis et al., 2009]. In June 2009, NASA launched the Lunar Reconnaissance Orbiter (LRO) carrying the Mini-RF synthetic aperture radar. This instrument has the ability to obtain images in the S band and the C band (4.2 cm), at resolutions of 150 (baseline) and

30 m (zoom) at both wavelengths. From July to September 2009, while the spacecraft was still in its elliptical commissioning orbit, the Mini-RF instrument acquired pre-impact S-zoom mosaics of all the LCROSS target craters, including Cabeus crater.

[7] We report here on the results of the SAR observations of Cabeus crater by Chandrayaan-1 and LRO. In section 2, we discuss the CPR measurements over Cabeus crater and identify the location of the LCROSS impact site in S-zoom images taken after October 9. In section 3, we discuss the implications of these observations for the nature of polar volatiles.

2. Observations

2.1. Circular Polarization Ratio

[8] The Mini-RF instrument is a dual-polarized synthetic aperture radar, which transmits in circular polarization (left-hand polarization for both instruments) and receives two coherent orthogonal linear polarizations (H and V). To calculate the circular polarization ratio of the received signal (CPR = SC/OC), we must be able to calculate the total power returned in the same polarization as was transmitted (SC = $|E_L|^2$) and the total power returned in the opposite polarization (OC = $|E_R|^2$). These values can be expressed in terms of the Stokes vector, which represents the time-averaged polarization properties of the backscattered field [Born and Wolf, 1980]. It is a straightforward matter to determine the Stokes vector from the total power received in the H and V channels and the real and imaginary parts of their complex conjugate, HV^* [Raney, 2006]. Circular polarization ratios can then be calculated from the Stokes vectors. For example, $CPR = SC/OC = (S_1 - S_4)/(S_1 + S_4)$, where S_1 represents the total received power, $S_1 = \langle |E_H|^2 + |E_V|^2 \rangle = \langle |E_L|^2 + |E_R|^2 \rangle$, and $S_4 = 2 \text{Im} \langle E_H E_V^* \rangle = \langle |E_L|^2 - |E_R|^2 \rangle$. The Forerunner and Mini-RF instruments were independently calibrated in-flight to correct for any offsets in radar gain and phase by transmit and receive experiments conducted with ground-based facilities (Arecibo and Green Bank radio observatories) [McKerracher et al., 2010].

[9] Two separate S band SAR mosaics of the lunar south pole have been obtained from lunar orbit. The first was obtained at 150 m resolution by the Forerunner instrument on Chandrayaan-1 during its first imaging season, from February to April 2009. The second was obtained at 30 m resolution by the Mini-RF instrument during LRO’s commissioning phase, from June to September 2009. The Forerunner instrument was fixed at a look angle of 32° , while the Mini-RF instrument is fixed at a look angle of 48° . Since both Chandrayaan-1 and LRO follow near-polar orbits, these side-looking radars are unable to see within $\sim 1^\circ$ – 2° of the lunar pole. Occasionally, the spacecraft will roll to obtain observations closer to the pole, but these opportunities are rare, so polar gaps are present in these mosaics.

[10] Circular polarization ratios were derived for both polar mosaics and plotted over the SC radar return (the quadrant covering Cabeus crater is shown in Figure 1). Note that the LRO images were processed with a pixel size of 15 m, each with an effective number of looks of ~ 4 . The images were then mosaicked with a pixel size of 50 m, yielding an ~ 44 -look average value for each location and an

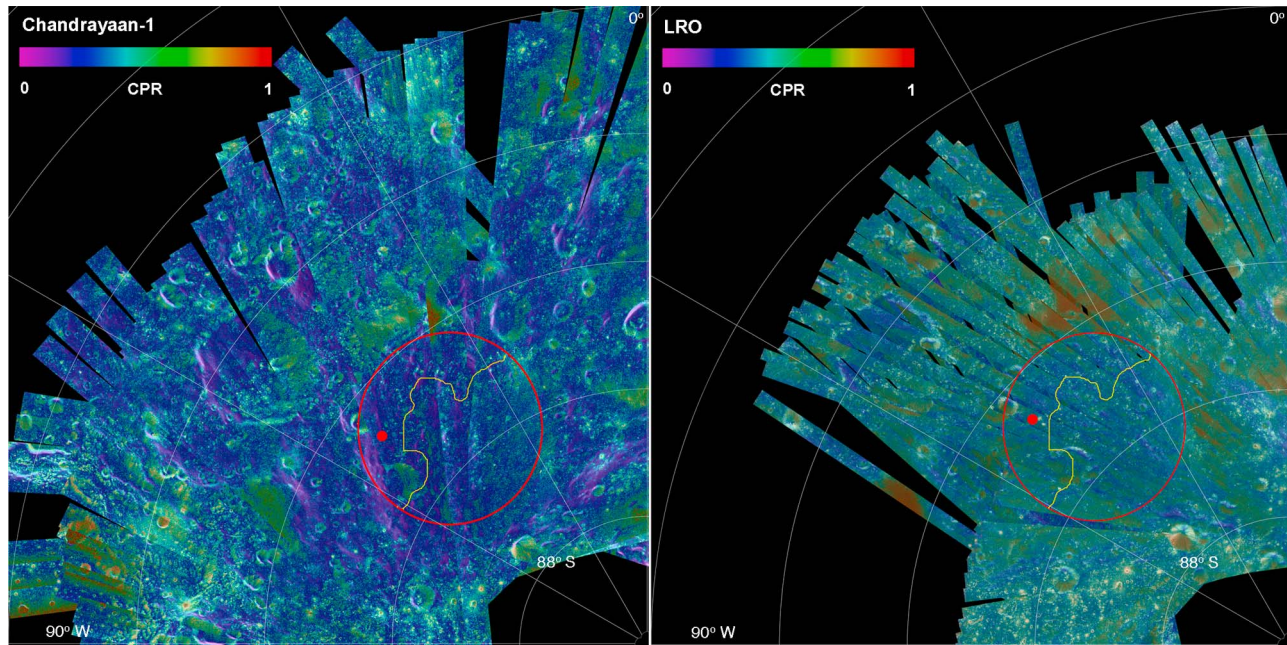


Figure 1. Circular polarization ratio (CPR) overlain on same sense (SC) S band radar mosaics of Cabeus crater taken by the Mini-RF instrument on (left) Chandrayaan-1 and (right) LRO. The thin red circle outlines the inner rim crest of Cabeus crater, the solid red disk represents the approximate location of the LCROSS impact, and the yellow line marks the southern extent of the area of shadow within Cabeus crater at the time of the LCROSS impact [Stubbs *et al.*, 2010]. The CPR values span the color spectrum from purple through red for values between 0 and 1. CPR values greater than 1 are assigned the color red. Note the relatively low values of CPR in the region of the impact.

approximate uncertainty $1/N^{1/2}$ of ± 0.15 in CPR [Campbell, 2002]. The C1 images had an effective number of looks of ~ 8 , for an approximate uncertainty of ± 0.35 in CPR. Both mosaics show Cabeus crater to have a CPR that is comparable to or lower than the average of nearby terrain in the southern lunar highlands (Figure 2). In the Chandrayaan-1 mosaic, Cabeus has a mean CPR = 0.25 ± 0.12 , lower than the CPR for the entire south polar mosaic, CPR = 0.31 ± 0.17 . In the LRO mosaic, Cabeus has a mean CPR = 0.38 ± 0.23 , also lower than the CPR for the entire south polar mosaic, CPR = 0.48 ± 0.30 . (Here, the error bars represent the variation in CPR over Cabeus.) In the C1 mosaic, only 0.01% of the pixels in Cabeus crater have CPR values greater than 1; in the LRO mosaic, only 2% of pixels have CPR values greater than 1. This is not consistent with the presence of thick deposits of water ice in Cabeus. There is also no noticeable change in CPR between the illuminated portion of the crater and the shadowed portion of the crater, where ice would be stable.

[11] Note that the CPR values obtained by Forerunner are ~ 0.1 smaller than those obtained by Mini-RF over the same region of the lunar surface. This is likely a result of the larger incidence angle of Mini-RF compared to Forerunner. For example, the CPR values of pyroclastic deposits have been shown to decrease as incidence angle decreases [e.g., Campbell *et al.*, 2009; Carter *et al.*, 2009]. Empirical backscatter models developed from 24 cm radar echoes of lava flows in Hawaii also predict an increase in CPR with increasing incidence angle [Campbell, 2009]. This trend is expected since more of a specular (and, hence, opposite

sense) component is returned at lower incidence angles, reducing the CPR.

[12] Campbell *et al.* [2006] previously imaged the south pole of the Moon at the S band using the Arecibo/Green Bank Telescope bistatic radar system. Given its viewing orientation from the Earth (with incidence angles $> 80^\circ$), portions of the pole, including a large part of the northern half of Cabeus crater, were shadowed from the radar. Still, those portions of Cabeus visible from Arecibo display remarkably low values for CPR (~ 0.1 – 0.2), consistent with the Mini-RF observations reported here.

[13] High CPR values are observed to the north of Cabeus (Figure 1), but this is not indicative of ice; rather it is indicative of a rough, rocky crater rim. Circular polarization ratios greater than 1 have been observed in other dry, rocky areas, such as Maxwell Montes on Venus [Campbell *et al.*, 1999] and blocky lava flows on the Earth [Campbell *et al.*, 1993]. CPR may increase in such regions due to double-bounce scattering between the surface and rock faces, but how such a mechanism can lead to CPR > 1 is unclear [Campbell *et al.*, 2009].

2.2. Impact Site

[14] Given its ability to image permanently shadowed regions, Mini-RF is one of a few instruments that are capable of placing the LCROSS impact site in a meaningful geologic context. Mini-RF obtained several images of the LCROSS impact site prior to October 9 in LRO's elliptical commissioning orbit. Mini-RF also imaged the impact site after October 9, from both west-looking (orbit 1435 on

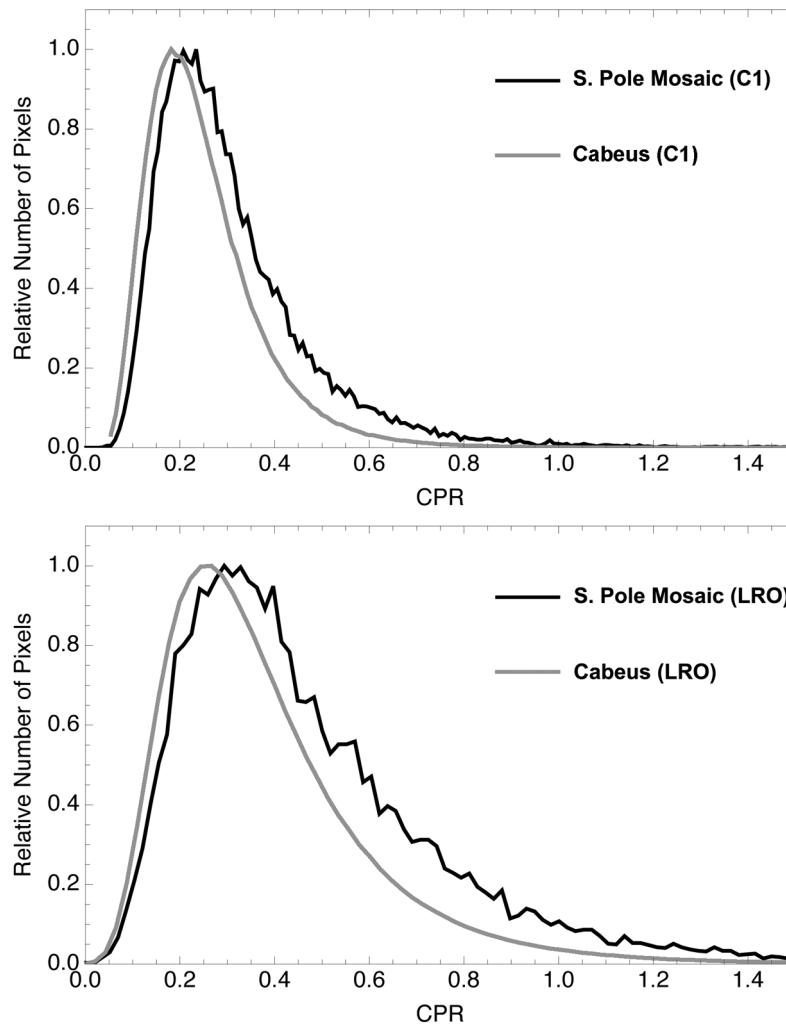


Figure 2. CPR values for Cabeus crater compared to the entire south polar mosaic for (top) Chandrayaan-1 and (bottom) LRO. The observed differences in CPR are likely due to the different look angles of the two instruments, 32° for Chandrayaan-1 and 48° for LRO.

19 October 2009) and east-looking orientations (orbit 3391 on 22 March 2010), in LRO's circular orbit. These data present an opportunity to search for changes consistent with a newly formed impact crater. In the commissioning orbit, Mini-RF had a resolution of 30 m; in the circular orbit, Mini-RF has a resolution of 15 by 30 m. The impactor was predicted to make a crater ~ 15 m in diameter [Korycansky *et al.*, 2009]. This puts the crater just at the limit of the instrument's resolution.

[15] To determine if Mini-RF would be likely to see the LCROSS impact site, we made a targeted observation of other man-made impact sites on the Moon. The best analogue to the LCROSS impact would be those craters formed by Apollo Lunar Module (LM) ascent stages, since they had masses similar to that of the Centaur upper stage used as the LCROSS projectile. Unfortunately, LM impact craters have yet to be identified in either Mini-RF or Lunar Reconnaissance Orbiter Camera (LROC) Narrow Angle Camera (NAC) images of the lunar surface. Instead, we searched for craters made by the somewhat more massive Apollo S-IVB upper stage, which had a dry mass of $\sim 14,000$ kg, compared

to the ~ 2000 kg mass of the Centaur upper stage [Korycansky *et al.*, 2009]. Crater diameters D are proportional to energy E as $D \propto E^{1/4}$ [Melosh, 1989], so if the projectiles impacted with a similar velocity, we would expect these craters to be ~ 1.6 times larger than that formed by the LCROSS impactor.

[16] On 4 February 1971, the Apollo 14 S-IVB upper stage impacted at 8.09°S , 26.02°W , creating a crater ~ 35 m in diameter which was observed by the crew of Apollo 16 and the LROC NAC (Figure 3). Mini-RF observed the same site in its S-zoom mode, and it observed a bright crater ~ 30 m in diameter (Figure 3). We would expect this crater to have a continuous ejecta blanket, extending about one crater radius from the crater rim [Moore *et al.*, 1974], and this is seen in the LROC image. Ejecta is usually bright in S band radar, since it contains many decimeter-size rocks. Surfaces that are rough at the radar wavelength scatter more energy back toward the antenna, resulting in higher radar backscatter values than smooth surfaces, which scatter energy away from the antenna. Given that the crater size observed in Mini-RF data is roughly the same as the rim-to-rim diameter of the crater observed in the LROC image, we find

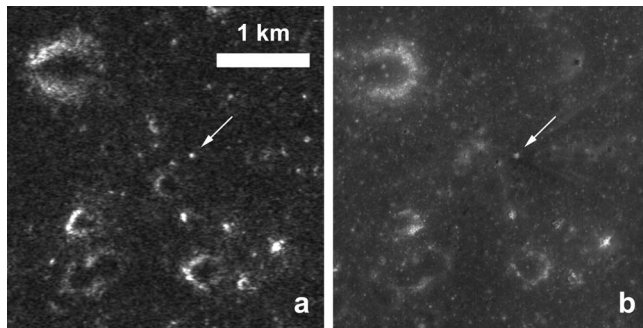


Figure 3. (a) S band radar image of the crater formed by the Apollo 14 S-IVB upper stage, which impacted the Moon on 4 February 4 1971 at 8.09°S , 26.02°W (LSZ_01776_2S1_EKU_15S334_V1.IMG). (b) LROC NAC image of the same region, taken at an incidence angle of 25° (M107049825RE.IMG).

that the ejecta blanket of this man-made impact is not easily observable in the SAR images (though a slight, diffuse brightening is seen to extend another 20–30 m from the crater). We may expect the LCROSS impact crater to exhibit similar properties. In this case, it may be difficult to observe the newly formed impact crater, as it will be at or below the resolution of Mini-RF. A radar-bright ejecta blanket would make the impact site more observable in the Mini-RF data.

[17] We registered our best preimpact S-zoom image with a postimpact image taken from the same viewing geometry near the impact position of 84.675°S , 48.703°W [Colaprete *et al.*, 2010]. We then registered these images to a near-infrared image taken by the LCROSS shepherding spacecraft approximately 4 s prior to impact, at an altitude of 10 km. Six features were identified in both images and were used to perform the registration. After the images were registered, more than 10 further features were found to be common to both images, giving confidence in the resulting registration (Figure 4).

[18] The location of the LCROSS impact crater has been determined by analysis of the expected trajectory of the Centaur impactor after its release from the shepherding spacecraft [W. Marshall *et al.*, The LCROSS impact location and image registration, manuscript in preparation, 2010]. Within the positional error bars, there is a small crater observed in the near-infrared image taken by the LCROSS shepherding spacecraft. As Mini-RF is able to “see in the dark,” registering these images to the Mini-RF S-zoom images allows us to put the LCROSS impact site in its broader geologic context. The impact site lies in what appears to be a rough crater ray, just northeast of a fresh ~ 1 km diameter crater. Outside of the bright crater ejecta, the site has the generally low radar return and CPR observed in most of Cabeus crater. Low radar return and CPR are indicative of a surface that is smooth and rock poor on the wavelength scale. For example, fine-grained deposits that are easily penetrable by radar, and have few embedded blocks (such as pyroclastic deposits), generally have low radar backscatter and CPR [e.g., Campbell *et al.*, 2008; Carter *et al.*, 2009].

[19] We note that at the impact position in the Mini-RF data there is a radar bright spot, which may in fact be the

LCROSS impact crater. However, given the resolution of our images, and the placement of the impact location, we are unable to confirm this identification. The candidate impact site lies on top of a bright crater ray, and the difference between the preimpact and postimpact images is comparable to the speckle noise seen in the original images, so the bright spot may simply represent a preexisting boulder or impact crater (Figure 5). Indeed, the entire differenced image shows little signal above the speckle noise.

[20] Several possibilities could account for this lack of detection in the differenced image. Mini-RF has a resolution of 30 m, so it is possible that the impact crater is simply less than 30 m in size, a value consistent with preimpact predictions. However, the radar backscatter for small craters should be enhanced due to the large amount of blocky ejecta excavated from the crater, allowing for detection of craters of less but comparable size to the image resolution. Thus, it is also possible that the impact did not excavate more decimeter-size blocks than were already present at the impact site. There may have already been many decimeter-size rocks present at the impact site, consistent with its location within a crater ray, or there may not have been much blocky ejecta excavated during the impact. If we assume the Centaur made a final crater ~ 20 m in diameter, then the transient crater diameter was $D_t = 0.84D = 17$ m, and the excavation depth was $\text{Hexc} \sim (1/10)D_t \sim 2$ m

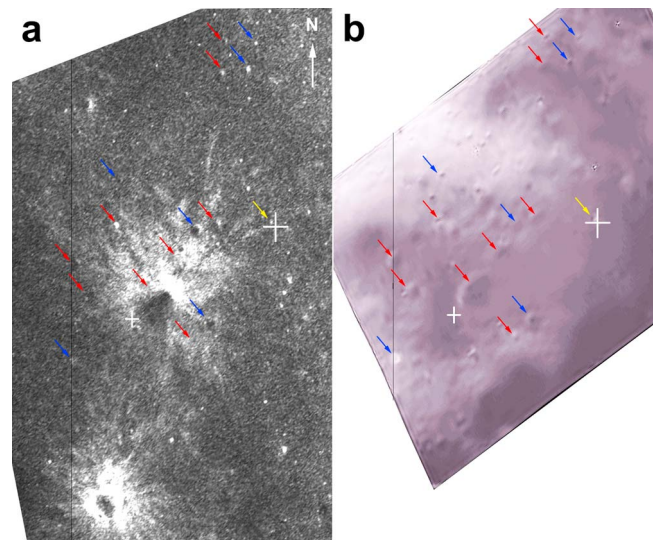
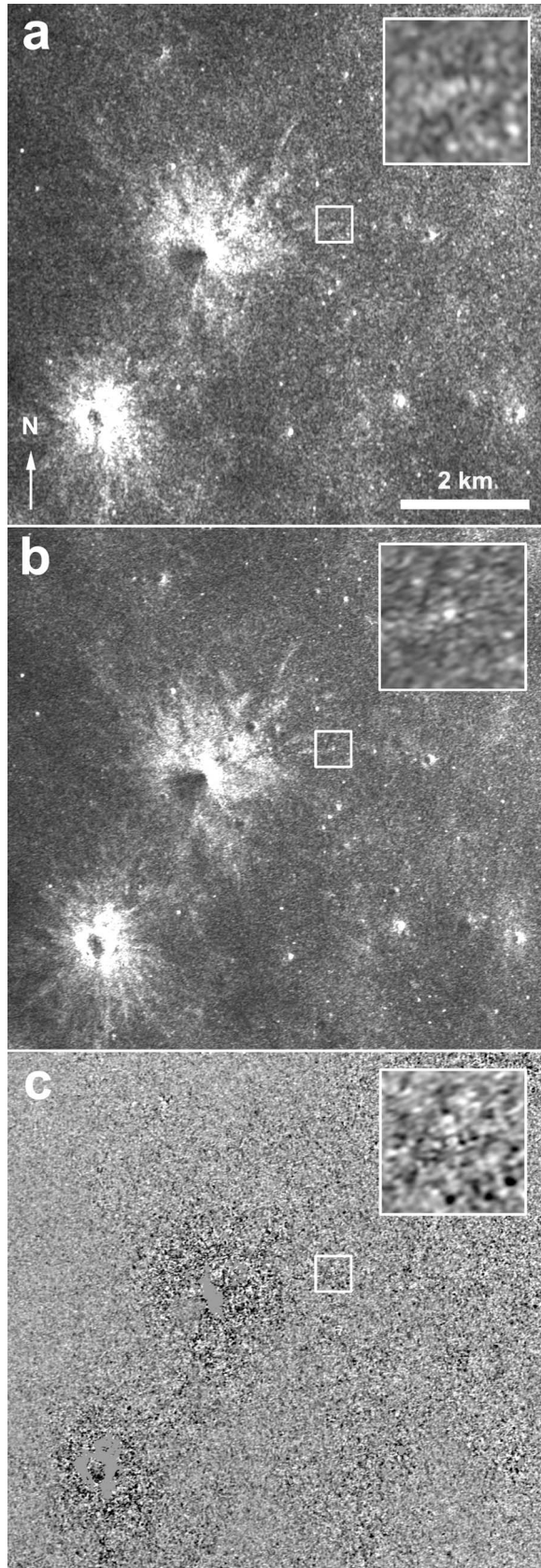


Figure 4. (a) Postimpact Mini-RF S-zoom image of the floor of Cabeus crater (LSZ_03391_2S1_OKU_85S318_V1.IMG, acquired on 22 March 2010), registered to (b) an NIR image taken by the LCROSS shepherding spacecraft (SSC) 4 s prior to impact (Cam6_W0000_T3460653m481). White crosses indicate the position of the Centaur impact (right) and the shepherding spacecraft impact (left), with error bars indicating the 3-sigma uncertainty in the trajectory (~ 420 m for the Centaur and ~ 225 m for the SSC). Blue arrows indicate features that were used to register the two images; red arrows indicate features that were consequently found to align after the images were registered. A radar bright spot is seen at the position of the Centaur impact (marked by a yellow arrow). The radar look direction is from the bottom left.



[Melosh, 1989]. Thus, the regolith at the LCROSS impact site might be block poor in the upper few meters, consistent with the low radar backscatter and CPR of the region.

3. Implications for Polar Volatiles

[21] Given the unique radar properties of thick deposits of ice, the Mini-RF observations provide constraints on the form of water discovered by LCROSS [Colaprete et al., 2010]. Since we see no CPR enhancements with Mini-RF at the LCROSS impact site, the water cannot be present as a thick deposit of ice, at least in the depths sampled by the radar.

[22] The penetration depth of a radar signal is dependent on its illuminating wavelength, λ , the loss tangent of the regolith, $\tan \delta$, and the real dielectric constant of the regolith, ϵ' [Campbell and Campbell, 2006]. To first order, the probing length is given by $\lambda/(2\pi\epsilon'^{1/2} \tan \delta)$. The loss tangent of highlands material ranges from 0.01 to 0.001, and the regolith has an average dielectric constant of ~ 3 [Carrier et al., 1991]. This gives a penetration depth of ~ 1 – 10 m for S band radar. The LCROSS impactor sampled materials to an excavation depth of ~ 2 m. This is roughly the same depth sampled by the radar. Even if the crater was somewhat larger, just below the resolution of Mini-RF at ~ 30 m, it would have an excavation depth only marginally larger, ~ 2.5 m. This is still within the depths observable by radar.

[23] Therefore, the icy materials detected by the LCROSS infrared spectrometer are unlikely to represent the shattered pieces of a decimeter to meter thick ice deposit, but instead are more likely present as small grains ($< \sim 10$ cm in size) mixed into the regolith, or a thin coating of ice on rock grains. It is possible that ice is present deep within the lunar regolith, at depths not directly observable with LCROSS or Mini-RF (i.e., more than several meters deep). However, this is unlikely due to the long time scales required to build up ice in permanently shadowed regions. Crider and Vondrak [2003] estimate that water would be present in only the top 1.6 m of an initially dry lunar regolith after 1 Ga. The sudden onset of thick ice at depth is also not supported by 70 cm Earth-based data, which can probe as much as tens of meters below the surface and shows low CPR on the floor of Cabeus crater [Campbell and Campbell, 2006].

[24] Lunar Prospector observed a reduction in the epithermal neutron count within Cabeus crater, which is suggestive of elevated levels of hydrogen atoms within the crater [Feldman et al., 1998]. If the hydrogen is in the form of water molecules, the results from Lunar Prospector suggest

Figure 5. Likely impact location of the LCROSS Centaur upper stage on the floor of Cabeus crater. (a) A “before” image taken on 1 August 2009 in LRO’s elliptical commissioning orbit, with a resolution of 30 m (LSZ_00455_2S1_OKU_87S324_V1.IMG). (b) An “after” image taken on 22 March 2010 in LRO’s circular prime mission orbit, with a resolution of 15 m (LSZ_03391_2S1_OKU_85S318_V1.IMG). (c) The difference between the two registered images. The impact location is outlined in white, and an inset at top right shows a close-up centered on the region of interest. The radar look direction is from the bottom left.

an ice concentration of 1.5 ± 0.8 wt% in the upper meter of the lunar regolith [Feldman *et al.*, 2001]. Such a concentration could account for the positive water detection by LCROSS, and the negative ice detection by Mini-RF, since deposits of ice capable of producing enhanced radar returns would also yield much higher hydrogen concentrations.

4. Conclusions

[25] Radar instruments on board Chandrayaan-1 and LRO observed Cabeus crater at the S band prior to the LCROSS impact. The circular polarization ratio of the top ~ 1 –10 m of the lunar regolith in Cabeus crater is comparable to or lower than the average of nearby terrain in the southern lunar highlands, in both the illuminated and permanently shadowed portions of the crater. In addition, $<2\%$ of the pixels in Cabeus crater have CPR values greater than 1. These results are not consistent with the presence of thick deposits of nearly pure water ice within a few meters of the lunar surface. The water observed by LCROSS must therefore be in the form of small (<10 cm), discrete pieces of ice mixed into the regolith, or a thin coating of ice on rock grains, forms of water not easily detectable by radar.

[26] In addition, Mini-RF on LRO acquired a postimpact S band image of the region surrounding the LCROSS impact site, providing important geologic context for the site. Registering the LRO image to a NIR image taken by the LCROSS shepherding spacecraft, we find that the impactor landed in the ray of a fresh, radar-bright, 1 km crater in an otherwise radar dark, low CPR area. Given the limited resolution of Mini-RF, the difference between pre-impact and postimpact images is comparable to the speckle noise seen in the original images. This implies that the size of the LCROSS impact crater is less than Mini-RF's resolution (30 m), consistent with preimpact predictions, and/or that the impact did not excavate more decimeter-size blocks than were already present at the impact site.

[27] **Acknowledgments.** We thank the Chandrayaan-1 and LRO projects for their efforts in returning the data presented here, and the Mini-RF science team for its efforts in reducing the data to its final, calibrated form. This work was supported by the LRO project, under contract with NASA. The authors would also like to thank Bruce Campbell and one anonymous reviewer, whose comments helped to improve the manuscript.

References

Arnold, J. R. (1979), Ice in the lunar polar regions, *J. Geophys. Res.*, *84*, 5659–5668.

Born, M., and E. Wolf (1980), *Principles of Optics*, Pergamon, New York, N. Y.

Campbell, B. A. (2002), *Radar Remote Sensing of Planetary Surfaces*, Cambridge Univ. Press, Cambridge, U. K.

Campbell, B. A. (2009), Scale-dependent surface roughness behavior and its impact on empirical models for radar backscatter, *IEEE Trans. Geosci. Remote Sens.*, *47*, 3480–3488, doi:10.1109/TGRS.2009.2022752.

Campbell, B. A., and D. B. Campbell (2006), Regolith properties in the south polar region of the Moon from 70-cm radar polarimetry, *Icarus*, *180*, 1–7, doi:10.1016/j.icarus.2005.08.018.

Campbell, B. A., R. E. Arvidson, and M. K. Shepard (1993), Radar polarization properties of volcanic and playa surfaces: Applications to terrestrial remote sensing and Venus data interpretation, *J. Geophys. Res.*, *98*, 17,099–17,113.

Campbell, B. A., D. B. Campbell, and C. H. DeVries (1999), Surface processes in the Venus highlands: Results from analysis of Magellan and Arecibo data, *J. Geophys. Res.*, *104*, 1897–1916.

Campbell, B. A., L. M. Carter, B. R. Hawke, D. B. Campbell, and R. R. Ghent (2008), Volcanic and impact deposits of the Moon's Aristarchus

Plateau: A new view from Earth-based radar images, *Geology*, *36*, 135–138, doi:10.1130/G24310A.1.

Campbell, B. A., B. R. Hawke, and D. B. Campbell (2009), Surface morphology of domes in the Marius Hills and Mons Rümker regions of the Moon from Earth-based radar data, *J. Geophys. Res.*, *114*, E01001, doi:10.1029/2008JE003253.

Campbell, D. B., B. A. Campbell, L. M. Carter, J.-L. Margot, and N. J. S. Stacy (2006), No evidence for thick deposits of ice at the lunar south pole, *Nature*, *443*, 835–837, doi:10.1038/nature05167.

Carrier, W. D., G. R. Olhoeft, and W. Mendell (1991), Physical properties of the lunar surface, in *Lunar Sourcebook*, edited by G. Heiken, pp. 475–566, Cambridge Univ. Press, Cambridge, U. K.

Carter, L. M., B. A. Campbell, B. R. Hawke, D. B. Campbell, and M. C. Nolan (2009), Radar remote sensing of pyroclastic deposits in the southern Mare Serenitatis and Mare Vaporum regions of the Moon, *J. Geophys. Res.*, *114*, E11004, doi:10.1029/2009JE003406.

Colaprete, A., et al. (2010), Water and more: An overview of LCROSS impact results, paper presented at the 41st Lunar and Planetary Science Conference, Lunar and Planet. Inst., The Woodlands, Tex.

Crider, D. H., and R. R. Vondrak (2003), Space weathering effects on lunar cold trap deposits, *J. Geophys. Res.*, *108*(E7), 5079, doi:10.1029/2002JE002030.

Feldman, W. C., S. Maurice, A. B. Binder, B. L. Barraclough, R. C. Elphic, and D. J. Lawrence (1998), Fluxes of fast and epithermal neutrons from Lunar Prospector: Evidence for water ice at the lunar poles, *Science*, *281*, 1496–1500.

Feldman, W. C., et al. (2001), Evidence for water ice near the lunar poles, *J. Geophys. Res.*, *106*, 23,231–23,251.

Hagfors, T., I. Dahlström, T. Gold, S.-E. Hamran, and R. Hansen (1997), Refraction scattering in the anomalous reflections from icy surfaces, *Icarus*, *130*, 313–322, doi:10.1006/icar.1997.5844.

Hapke, B. (1990), Coherent backscatter and the radar characteristics of outer planet satellites, *Icarus*, *88*, 407–417, doi:10.1016/0019-1035(90)90091-M.

Harmon, J. K., P. J. Perillat, and M. A. Slade (2001), High-resolution radar imaging of Mercury's north pole, *Icarus*, *149*, 1–15, doi:10.1006/icar.2000.6544.

Korycansky, D. G., C. S. Plesko, M. Jutzi, E. Asphaug, and A. Colaprete (2009), Predictions for the LCROSS Mission, *Meteorit. Planet. Sci.*, *44*, 603–620.

Lanzerotti, L. J., W. L. Brown, and R. E. Johnson (1981), Ice in the polar regions of the Moon, *J. Geophys. Res.*, *86*, 3949–3950.

McKerracher, P. L., et al. (2010), Mini-RF calibration, a unique approach to on-orbit synthetic aperture radar system calibration, paper presented at the 41st Lunar and Planetary Science Conference, Lunar and Planet. Inst., The Woodlands, Tex.

Melosh, H. J. (1989), *Impact cratering*, Oxford Univ. Press, Oxford, U. K.

Moore, H. J., C. A. Hodges, and D. H. Scott (1974), Multi-ringed basins: Illustrated by Orientale and associated features, *Proc. Lunar Sci. Conf.*, *Vth*, *1*, 71–100.

Morgan, T. H., and D. E. Shemansky (1991), Limits to the lunar atmosphere, *J. Geophys. Res.*, *96*, 1351–1367.

Muhleman, D. O., B. J. Butler, A. W. Grossman, and M. A. Slade (1991), Radar images of Mars, *Science*, *253*, 1508–1513, doi:10.1126/science.253.5027.1508.

Nozette, S., C. L. Lichtenberg, P. Spudis, R. Bonner, W. Ort, E. Malaret, M. Robinson, and E. M. Shoemaker (1996), The Clementine bistatic radar experiment, *Science*, *274*, 1495–1498.

Nozette, S. P., et al. (2010), The Lunar Reconnaissance Orbiter Miniature Radio Frequency (Mini-RF) technology demonstration, *Space Sci. Rev.*, *150*, 285–302, doi:10.1007/s11214-009-9607-5.

Ostro, S. J., D. B. Campbell, R. A. Simpson, R. S. Hudson, J. F. Chandler, K. D. Rosema, I. I. Shapiro, E. M. Standish, R. Winkler, and D. K. Yeomans (1992), Europa, Ganymede, and Callisto: New radar results from Arecibo and Goldstone, *J. Geophys. Res.*, *97*, 18,227–18,244.

Paige, D. A., et al. (2010), Diviner lunar radiometer experiment: Early mapping mission results, paper presented at the 41st Lunar and Planetary Science Conference, Lunar and Planet. Inst., The Woodlands, Tex.

Peters, K. J. (1992), Coherent-backscatter effect: A vector formulation accounting for polarization and absorption effects and small or large scatterers, *Phys. Rev. B*, *46*, 801–812.

Raney, R. K. (2006), Dual-polarized SAR and Stokes parameters, *IEEE Geosci. Remote Sens. Lett.*, *3*, 317–319.

Slade, M. A., B. J. Butler, and D. O. Muhleman (1992), Mercury radar imaging: Evidence for polar ice, *Science*, *258*, 635–640, doi:10.1126/science.258.5082.635.

Spudis, P. D., et al. (2009), The Mini-SAR imaging radar on the Chandrayaan-1 Mission to the Moon, paper presented at the 40th

- Lunar and Planetary Science Conference, Lunar and Planet. Inst., The Woodlands, Tex.
- Spudis, P. D., et al. (2010), Initial results for the north pole of the Moon from Mini-SAR, Chandrayaan-1 mission, *Geophys. Res. Lett.*, *37*, L06204, doi:10.1029/2009GL042259.
- Stacy, N. J. S., D. B. Campbell, and P. G. Ford (1997), Arecibo radar mapping of the lunar poles: A search for ice deposits, *Science*, *276*, 1527–1530, doi:10.1126/science.276.5318.1527.
- Stubbs, T. J., Y. Wang, E. Mazarico, G. A. Neumann, D. E. Smith, M. T. Zuber, and M. H. Torrence (2010), Characterizing the optical shadowing at the Moon using LOLA topographic data: Predictions for the LCROSS impact, paper presented at the 41st Lunar and Planetary Science Conference, Lunar and Planet. Inst., The Woodlands, Tex.
- Thompson, T. W., E. A. Ustinov, and E. Heggy (2010), Modeling radar scattering from icy lunar regoliths, paper presented at the 41st Lunar and Planetary Science Conference, Lunar and Planet. Inst., The Woodlands, Tex.
- Watson, K., B. C. Murray, and H. Brown (1961), The behavior of volatiles on the lunar surface, *J. Geophys. Res.*, *66*, 3033–3045.
-
- D. B. J. Bussey, C. D. Neish, G. W. Patterson, and B. J. Thomson, Johns Hopkins University Applied Physics Laboratory, Laurel, MD 20723, USA. (catherine.neish@jhaupl.edu)
- L. M. Carter, NASA Goddard Space Flight Center, Greenbelt, MD 20770, USA.
- W. Marshall, Universities Space Research Association, Mountain View, CA 94043, USA.
- P. Spudis, Lunar and Planetary Institute, Houston, TX 77058, USA.